

## Rheological Investigation of Polyamide 6 TiO<sub>2</sub>- and BaSO<sub>4</sub>-Nanocomposites

Irene Hassinger, Thomas Burkhart

Department of Materials Science, Institute for Composite Materials, Institute for Composite Materials, Department of Materials Science, Technical University of Kaiserslautern, D-67663 Kaiserslautern, Germany

Correspondence to: I. Hassinger (E-mail: irene.hassinger@ivw.uni-kl.de)

**ABSTRACT:** Commercially available TiO<sub>2</sub> and BaSO<sub>4</sub> nanoparticles were incorporated in polyamide 6 (PA 6) via twin screw extrusion. The primary particle size of nanoparticles was 15 nm and 20 nm. The compounds were manufactured via multiple extrusion and dilution processing steps. The dispersion of the nanoparticles in the matrix was investigated by scanning electron microscopy and image analysis, micro-tomography, and transmission electron microscopy. The rheological properties were determined via plate–plate-rheometer. It was found that for TiO<sub>2</sub> fillers a threefold extrusion process is sufficient to realize a dispersion index of 94.4%. BaSO<sub>4</sub> fillers were hardly dispersible, ending up with a maximum dispersion index of 71%. Deagglomeration does not lead to a change in rheological properties but the number of extrusion steps decreases the rheological properties. A good particle-matrix interaction leads to higher moduli and viscosity. The remaining agglomerates seem to act as defects decreasing the energy absorption of the respective compounds. © 2012 Wiley Periodicals, Inc. *J. Appl. Polym. Sci.* 000: 000–000, 2012

**KEYWORDS:** extrusion; nanoparticles; nanowires and nanocrystals; rheology; polyamides

Received 5 March 2012; accepted 27 July 2012; published online

DOI: 10.1002/app.38412

### INTRODUCTION

Polymeric nanocomposites are of great scientific and technological interest due to their exceptional mechanical, thermal, and other properties achieved at very low nanoparticle content (<3 vol %).<sup>1</sup> Thus, they are very attractive due to their processability with traditional polymer processing equipment like extrusion.<sup>2</sup> The size of traditional reinforcements is in the micrometer range, but in case of nanoparticles at least one dimension is in the nanometer scale. Usually, inorganic reinforcements are added to enhance the stiffness and the yield stress due to strong interfacial strength.<sup>3</sup> Therefore, applications are yarns for sportswear and pantyhoses, protective equipment, and high quality plastic products like gear parts and gear wheels. The extraordinary properties of nanocomposites depend on their huge interfacial surface area. Thus, the interface/interphase properties may become the dominant part of the macroscopic behavior of the nanoparticle-modified polymer composites, changing also the molecular mobility of particles within polymer matrix. Furthermore, decreasing the particle size decreases also the average interparticle distance at constant volume fraction, leading to a potential network structure based on filler–filler interactions.<sup>1</sup> Because of their big intrinsic surface area, nanoparticles build up agglomerates. In case of low filler-matrix interaction, debonding occurs, which leads to microvoids as a function of

agglomerate size, where stress can concentrate. Only homogeneously distributed small particles (nanoscale) have the potential to increase toughness.<sup>3</sup>

It is possible to analyze the degree of dispersion via the analysis of the rheological behavior. A replacement of traditional composites, polymers and blends by nanocomposites, produced by melt processing techniques, is possible with reproducible processability and improvement in properties.<sup>1</sup>

The analytical techniques to analyze the dispersion of nanoparticles in polymers are electron microscopy [transmission electron microscopy (TEM)/scanning electron microscopy (SEM)], atomic force microscopy (AFM), and rheological measurements.<sup>4–6</sup> Accessing the processing characteristics, rheological studies are very important. Rheological behavior of polymer melts depends besides many factors on process parameters, molecular properties, and the flow geometry.<sup>7</sup> The nanocomposite structure highly affects the rheological behavior such as nature of polymer, molecular weight and particle distribution, particle-matrix interaction, including interfacial tension, and morphology.<sup>2,7,8</sup> Kharchenko et al.<sup>9</sup> showed an increase in viscosity of CNT filled polymers for low concentrations, and Ren and Krishnamoorti<sup>10</sup> showed this behavior also for clay nanocomposites. The behavior of polymer melts highly depends on the incorporation of dispersed particles.<sup>11</sup> On one hand, the  $G'$  and

$G''$ -moduli of the melt increase along the entire frequency range with stable curve progression.<sup>11</sup> Giannelis et al.<sup>8</sup> and Privalko et al.,<sup>12</sup> for example, found that in the low frequency range, where linear viscoelasticity dominates, the melt viscosity increases monotonically with increasing particle content independent of particle shape and incorporation method.<sup>1</sup> On the other hand, in case of a strong particle-matrix interaction, the curve progression can be changed, for example with the formation of a plateau at low frequencies dependent on the maximum packaging density.<sup>13</sup> Minagawa and White, for example, could demonstrate this behavior on a TiO<sub>2</sub>-HDPE composite<sup>14,15</sup> and Friedrich on silicate spheres coated with maleic anhydride-polystyrol in PS.<sup>16</sup> On the contrary, Jain et al.<sup>17</sup> reported a dramatic reduction of the viscosity of PP through the addition of a small amount of silica nanoparticles accounting this with a selective adsorption of high molar mass polymer chains on the nanoparticle surface. Especially, the interparticle distance overweighs the radius of gyration in case of getting smaller where confinement and bridging effects become evident.<sup>17</sup>


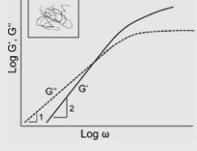
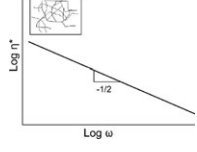
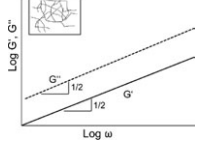
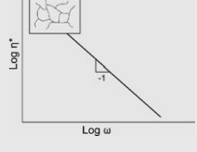
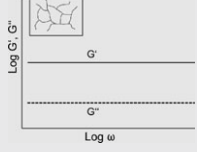
The characteristic mastercurves for linear macromolecules, gels, and networks are very different. The slopes of  $\log G'(\log \omega)$  and  $\log G''(\log \omega)$  in network structures are 0. The slope of the referring viscosity is  $-1$ . For gels, the slope of  $\log G'(\log \omega)$  and  $\log G''(\log \omega)$  are 0.5. The slope of the referring viscosity is  $-0.5$ .<sup>11</sup> In case of linear monodisperse polymers, the slope of  $G'$  and  $G''$  versus frequency, in the terminal region, is expected to be 2 and 1, respectively.<sup>18–20</sup> The slope of the viscosity  $\eta$  for linear polymers is 0.<sup>11</sup> The respective slopes including descriptions

are given in Table I. Network structures, physical or/and chemical ones, will be detected via the analysis of the rheological behavior. At low frequencies, polymer flowing will be enabled increasing the effect of polymer-particle interaction as a function of filler loading.<sup>21,22</sup> At lower strain levels a breakdown of filler-filler networks can be detected according to literature.<sup>7</sup> Linear and nonlinear viscoelastic properties in the molten state are generally useful to determine the degree of polymer-filler interactions and the structure-property relationship of the polymeric materials. As a result, rheology appears to be a unique technique for the study of polymer nanocomposites. It reveals important properties for extrusion processing, injection molding, or fiber spinning.

The aim of this work is to investigate the rheological properties of PA 6 nanocomposites as a function of different degrees of particle dispersion, particle loading, and extrusion steps. The reinforcement of the used filler and the polymer degradation during extrusion are two competing mechanisms producing nanocomposites. For polyamide, the main degradation mechanisms base on main-chain scission and cross-linking correlate well with the rheological behavior.<sup>2</sup>

The production of nanocomposites via masterbatch-process is a widely used technique to realize a well dispersion of nanoparticles within polymer matrix due to the high-shear energy input during extrusion. Various particle contents will be realized via dilution processing steps. Therefore, analysis of the respective

**Table I.** Description of Slope for  $G'$ ,  $G''$ , and  $\eta^*$ <sup>11,18–20</sup>

	Change in slope	Change in particle-polymer interaction and polymer branching
$G', G'' (\omega \rightarrow \infty)$	↑	↓
$\eta^* (\omega \rightarrow \infty)$	↓	↑
	↑	↑
	↓	↓
	Slope of $\log \eta^*(\log \omega)$ , $\log G'(\log \omega)$ , and $\log G''(\log \omega)$	
Linear macromolecules		
Gel		
Network		

**Table II.** Rheological Properties of all the Components of PA6 Unfilled and Filled with 7 vol % TiO<sub>2</sub> and BaSO<sub>4</sub> for Different Extrusion Steps as a Function of Frequency

Extrusion steps	No. particles/just PA6				Filler 7 vol % TiO <sub>2</sub>			BaSO <sub>4</sub>
	0	1	2	7	1	2	7	2
1.2 < ω < 1.6 rad/s								
Slope G'	0.752	0.251	0.65	0.86	0.626	0.682	0.703	0.883
Slope G''	0.786	0.991	0.968	0.943	0.949	0.933	0.912	0.984
Slope η*	-0.215	-0.011	-0.033	-0.059	-0.054	-0.071	-0.094	-0.015
79.2 < ω < 99.8 rad/s								
Slope G'	1.125	1.589	1.412	1.508	1.215	1.135	1.156	1.479
Slope G''	0.821	0.905	0.909	0.934	0.824	0.777	0.837	0.896
Slope η*	-0.159	-0.083	-0.083	-0.06	-0.159	-0.197	-0.148	-0.092

extrusion processing steps including dilution processing steps on the rheological properties is needed.

## EXPERIMENTAL

### Material

In case of PA 6, Ultramid B 24 N 03 from BASF, a commercially available light stabilized polyamide 6 grade for the production of textile fibers, especially suitable for high speed spinning, was used. The applied nanofiller was a commercially available titanium dioxide particle powder (Hombitec RM 300, Sachtleben Chemie GmbH) with an average primary particle size of 15 nm and an average specific surface area of 70 m<sup>2</sup>/g. The particle surface was functionalized with polyalcohol. The second nanofiller was a commercially available noncoated barium sulfate particle powder (Sachtoperse N 20, Sachtleben Chemie GmbH) with an average primary particle size of 20 nm and an average specific surface area of 60 m<sup>2</sup>/g. TiO<sub>2</sub> was chosen due to promising results in particle-matrix interaction and property enhancement with PA 6.6.<sup>23</sup> On the opposite, BaSO<sub>4</sub> was chosen because of the “naked” surface area. Here, the goal was to investigate the particle behavior having a high surface energy during melt extruding particles. Thus, the particle size and specific surface are kept constant. The application for such nanocomposites is ballistic protective helmets made of aramid and PA6-nanocomposite yarns with improved toughness.

### Extrusion

Before extrusion, PA 6 and particle powder were dried for 24 h at 80°C. In case of extrusion, a co-rotating twin screw extruder from Berstorff GmbH was used. The components were fed via high precision gravimetric feeders (K-tron Deutschland GmbH) through the main feeder to be processed at 220°C and 300 rpm. The string from a 4 mm die was cooled in a water bath, pelletized, dried, and injection-molded (Allrounder 320, Arburg GmbH) into test specimens for impact and tensile testing.

It has been shown<sup>2,23</sup> that iteration of extrusion process steps can enhance the deagglomeration of macroagglomerates. Therefore, a multiple-extrusion-process was applied. In a first step, a 7 vol % masterbatch (labeled: once extruded (1xex)) was produced and in a follow up of six further process steps the microparticles in the PA 6 were more and more deagglomerated and distributed [labeled: 2–7 extrusion steps (1xex (7 vol %) to 7xex (7 vol %))]. The masterbatch containing 7 vol % TiO<sub>2</sub>-nanoparticles with deagglomeration

and further dispersion and distribution after one extrusion steps were diluted down to 0–2 vol % nanoparticle content by the addition of neat PA 6 (labeled: two times (2xex (0–2 vol %))).

### Rheology

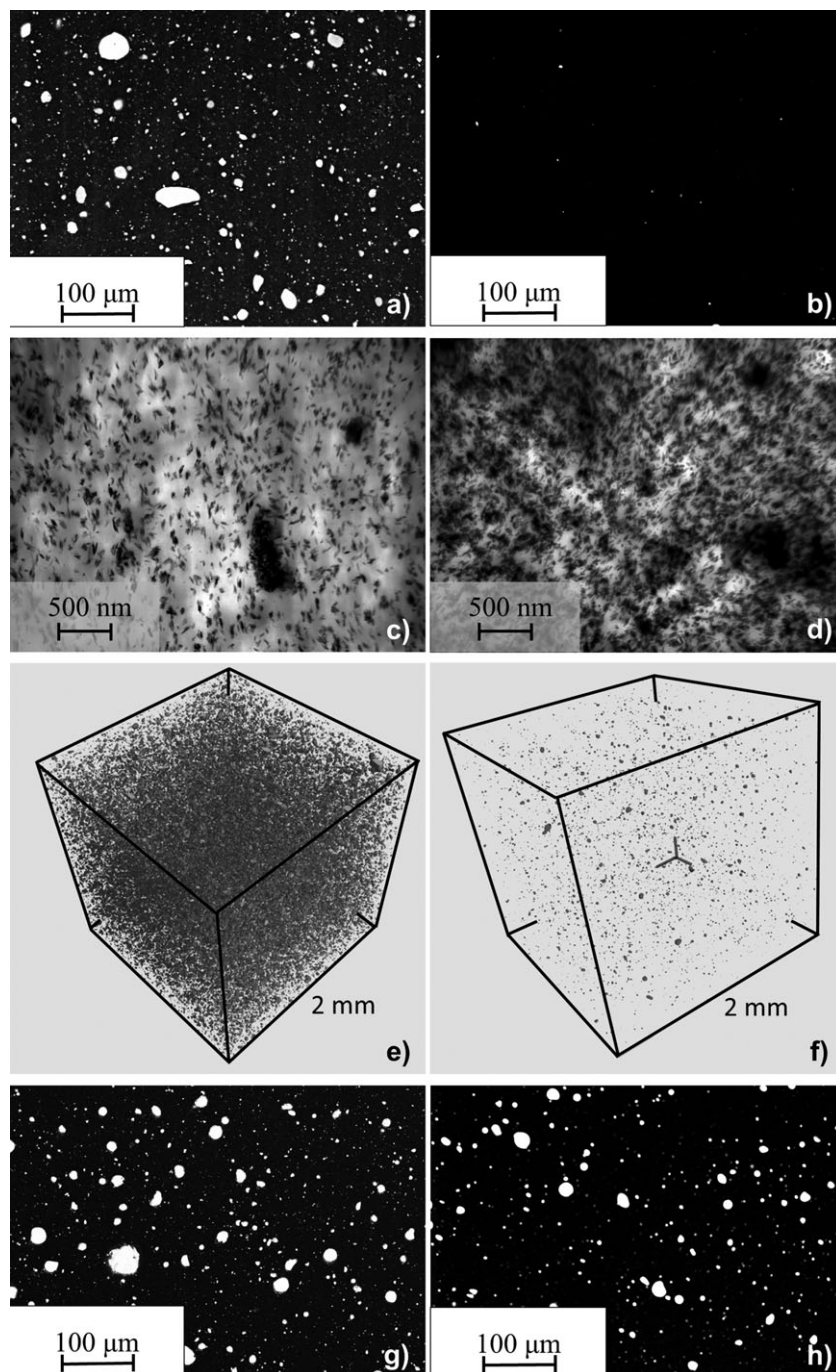
Oscillatory rheological measurements were executed in dynamic mode on a rheometer (ARES, Rheometric Scientific) equipped with parallel plate geometry (plate diameter 25 mm) at 220°C and under atmospheric conditions. Polymer nanocomposites disks with the dimensions 2 mm thickness and 25 mm in diameter were produced via compression molding. The size for the plate–plate configuration was thus 2 mm. Before molding and testing, the samples were dried for at least 24 h at 80°C. Dynamic frequency scan tests were performed for all samples at a strain amplitude of 10%, which is within the viscoelastic region as deducted from dynamic strain scan tests. These tests were performed at 220°C and with a frequency of 10 rad/s and 500 rad/s with a strain sweep from 0.1 to 100%. To check the stability of the PA used, time sweep tests were performed for 20 min (1200 s) at 500 rad/s, 10% strain, and 220°C temperature. The material is stable in this period of time. The frequency sweep tests last 243.2 s and thus are within this testing time. The frequency in the frequency sweep tests was chosen from 500 down to 1 Hz.

### Scanning Electron Microscopy and Analysis of Dispersion Index

Polished surfaces were analyzed using an electron microscope (Supra 40 from Zeiss and JSM 6300 from Joel) via detecting the backscattering electrons. Fracture surfaces were scanned with a secondary electron detector. All samples were coated with gold using a Sputtering Device (SCD—050, Balzer AG). The SEM-images were analyzed with an image analysis software by which the number of agglomerates and size were measured. From these results, the dispersion index was calculated according to eq. (1):<sup>24</sup>

$$D = 1 - f \times \frac{A}{A_{im} \times \phi_{nano}} \quad (1)$$

with  $D$  is the dispersion index,  $A$  is area of the agglomerates,  $A_{im}$  is area of the image,  $f$  is shape factor, and  $\phi_{nano}$  is volume fraction.



**Figure 1.** SEM (a, b), TEM (c, d), and  $\mu$ CT (e, f) images of 7 vol %  $\text{TiO}_2$ -nanoparticles (a–f) dispersed in a PA6 matrix after one (a, c, e) and seven (b, d, f) extrusion steps. SEM images of 7 vol %  $\text{BaSO}_4$ -nanoparticles dispersed in a PA6 matrix after one (g) and seven (h) extrusion steps.

#### Definition of the Shape Factor

The shape factor  $f$  will be calculated with a so called control compound containing a well-defined dispersion of particles based on a defined volume content. Therefore, we used a nano reinforced PA 6 composite with no dispersion which will be set to zero regarding dispersion index.  $f$  can be calculated by solving the eq. (2).

$$f = (1 - D) \times \frac{A_{im} \times \phi_{Nano}}{A} \quad (2)$$

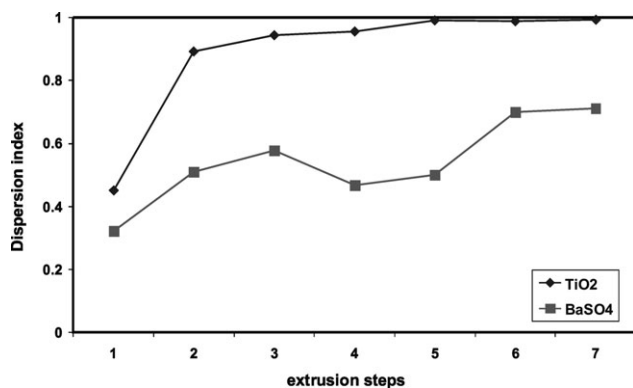
In our case,  $f$  was set to 0.63.

#### Computed Micro-Tomography System 3D

Computed micro-tomography ( $\mu$ CT) measurements were performed on a nanotom X-ray system of Phoenix X-ray Systems Services GmbH.

#### Transmission Electron Microscopy

TEM images were carried out on Philips EM 400 T TEM. Samples for the TEM analysis were embedded in resin before cutting 80–100-nm thick films with a Leica microtom (Leica EM UC6).



**Figure 2.** Dispersion index of 7 vol % TiO<sub>2</sub> and BaSO<sub>4</sub> masterbatches versus the number of extrusion steps.

### Mechanical Properties

Mechanical properties for these materials can be taken from Ref. 25.

### Gel Permeation Chromatography

Gel permeation chromatography (GPC) measurements were performed with a 1,1,1,3,3,3-hexafluoro-2-propanol (HFIP) eluent on the multiple extruded neat particle free PA 6 matrix to get the molecular weight distribution.

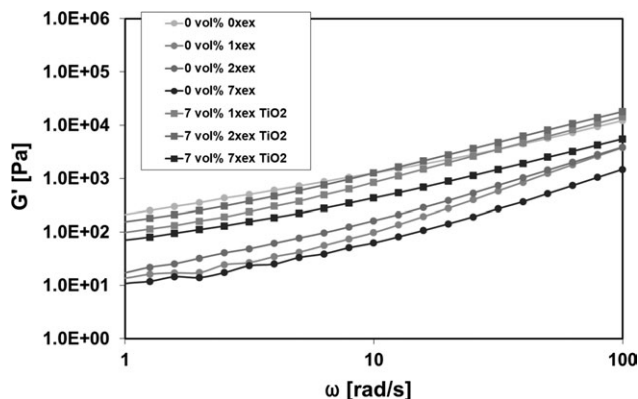
## RESULTS AND DISCUSSION

### General Influence of Multiple Extrusion Steps on Rheological Properties

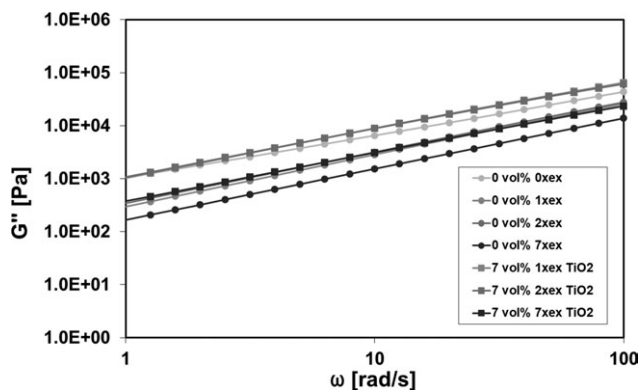
The interpretation of the rheological properties is based on Table I. The respective rheological properties of all the compounds as a function of frequency are evident from Table II.

### Morphological Analysis (SEM, TEM, $\mu$ CT) of Reinforced PA6 as a Function of Extrusion Steps

The higher the shear energy input the higher the potential of deagglomeration regarding top-down method, which will be realized via multiple extrusion processes.<sup>23,26,27</sup> To analyze the number of extrusion steps needed to realize a static state of deagglomeration, it was analyzed how material behaves in extruding up to several times, in our case seven times.



**Figure 3.**  $G'$  versus the frequency of neat PA6 and PA6 filled with 7 vol % TiO<sub>2</sub>-nanoparticles.

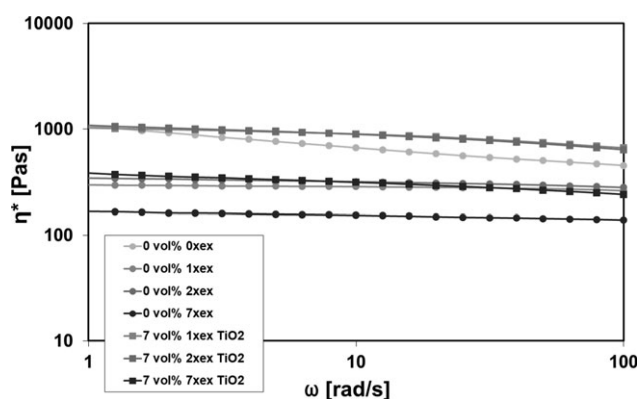


**Figure 4.**  $G''$  versus the frequency of neat PA6 and PA6 filled with 7 vol % TiO<sub>2</sub>-nanoparticles.

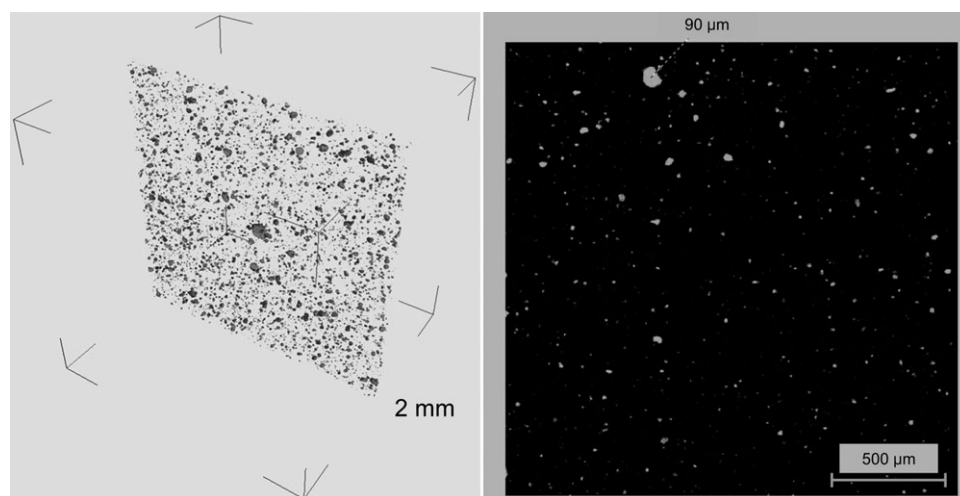
SEM images are given in Figure 1(a, b, g, h). Results for TiO<sub>2</sub>-deagglomeration are given in Figure 1(a, b) and for BaSO<sub>4</sub>-nanoparticle deagglomeration are given in Figure 1(g, h). Figure 1(a, g) gives the TiO<sub>2</sub> and BaSO<sub>4</sub> dispersion quality after one extrusion step, Figure 1(b, h) after seven extrusion steps.

The SEM images show a bad degree of deagglomeration for both masterbatches, TiO<sub>2</sub> (a) and BaSO<sub>4</sub> (g), after one extrusion step. Deagglomeration depends on the interchanges particle to matrix and Van der Waals interchanges of particles itself. BaSO<sub>4</sub> filled material is less deagglomerated than TiO<sub>2</sub> filled materials which will be also not improved with further extrusion steps (h), where still big agglomerates can be detected. On contrary, TiO<sub>2</sub>-compounds show a very good degree of deagglomeration. After seven extrusion steps, only agglomerates less than 1  $\mu$ m in size will be found (b).

Based on the SEM findings including image analysis, the respective dispersion indices were calculated according to eq. (2) (Figure 2). TiO<sub>2</sub>-masterbatches start with a very small dispersion index of 45.1% after one extrusion step but already after the second one the dispersion index increases up to 89.2%, after the third one up to 94.4%, and after the fifth extrusion step 99% was reached. In case of BaSO<sub>4</sub>-PA 6-compounds, the maximum dispersion index is in the range of 70% after the sixth and seventh extrusion steps coming from 32.2% after the first one.



**Figure 5.** Viscosity dependence on frequency for neat PA6 and PA6 filled with 7 vol % TiO<sub>2</sub>-nanoparticles.



**Figure 6.**  $\mu$ CT-3D-images cut into slices for once extruded 7 vol %  $\text{TiO}_2$  nanocomposites. The path from a 3D to the 2D image is given.

Figure 1(e, f) shows the  $\mu$ -CT-3D-analysis illustrating the bad degree of deagglomeration for  $\text{TiO}_2$  reinforced PA 6 compounds, once extruded in comparison with seven times extruded.

Figure 1 shows the TEM images of nanoparticles dispersed in the PA 6 matrix after one (c) and seven (d) extrusion steps with their needle like shape. After one extrusion step [Figure 1(c)], almost all nanoparticles will be found as agglomerates. Only few nanoparticles are found as primary particles dispersed in polymer matrix. After seven extrusion steps [Figure 1(d)], most of the particles will be detected as nanoparticles dispersed in the matrix only few particles are still located as agglomerates.

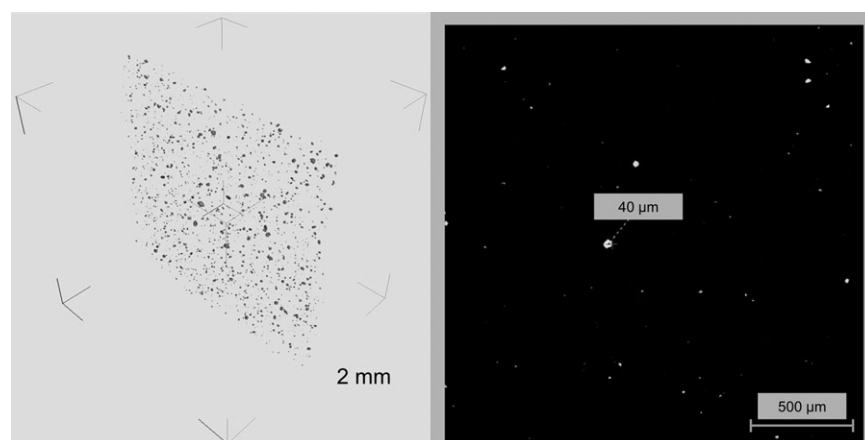
According to GPC results, the molecular weight (Figure 8) is reduced by 16.75%: from 73.98 kg/mol (0 extrusion steps) to 61.59 kg/mol (7 extrusion steps). This reduction, originated by main-chain scission mechanism promoted by the shear stresses and residence time in the twin-screw extruder, leads also to a reduction in rheological properties as shown in Figures 3–5. In Figures 6 and 7, one can see  $\mu$ -CT-3D-images cut into slices. The path from a 3D to the 2D image is given. The comparison of the 2D-image taken from the  $\mu$ -CT-3D-analysis with the

SEM-images illustrates less detected agglomerates in case of  $\mu$ -CT. This reveals an optimistic view via  $\mu$ -CT on once and seven times extruded material where still agglomerates can be found.

#### Rheological Properties ( $G'$ , $G''$ , and $\eta^*$ vs. $\omega$ ) as Function of Extrusion Steps (0, 1, 2, 7) of just PA6 and the Resulting Molecular Build-Up

Figures 3–5 show the rheological behavior, expressed in  $G'(\omega)$  and  $G''(\omega)$  and  $0^*(\omega)$ , respectively, of multiple extruded neat PA6 after 1, 2, and 7 extrusion steps as a function of frequency. The molded neat polyamide matrix is labeled as 0xex.

The  $G'$  versus  $\omega$  (Figure 3) as well as  $G''$  versus  $\omega$  (Figure 4) for the neat matrix generally decreases with increasing number of extrusion steps.  $G'$  increases from the first to the second extrusion step and strongly decreases to the seventh extrusion step. The  $G''$  modulus does not show this increase in modulus, but the curve progression remains almost the same from the first to the second extrusion step. The slope, one key factor for intrinsic interaction, runs through a maximum after two extrusion steps in the high frequency range.



**Figure 7.**  $\mu$ CT-3D-images cut into slices for once extruded 7 vol %  $\text{TiO}_2$  nanocomposites. The path from a 3D to the 2D image is given.

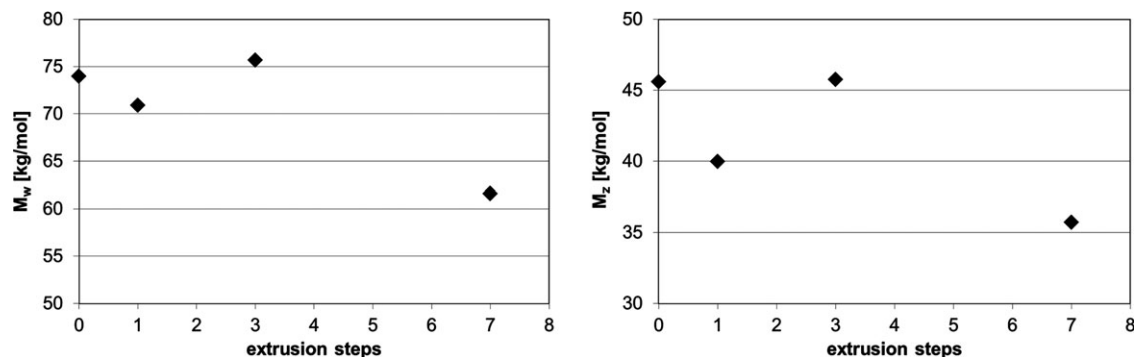


Figure 8. Mean molar mass ( $M_w$  and  $M_z$ ) for neat PA6 versus number of extrusion steps.

In Figure 5, we observe that the complex viscosity,  $\eta^*$ , of PA6 is about four times higher than  $\eta^*$  of seven times extruded PA6. In between, the viscosity is increased from the first to the second extrusion step.

Figure 8 reveals the molecular weight of neat multiple extruded PA6. The molecular weight decreases from the first to the second extrusion steps but increases again to the third extrusion step. This can be due to cross linking. After seven extrusion steps, the polymer chains are degraded.

The reduced  $G'$  and  $G''$  moduli occur due to polymer degradation. The viscosity is reduced with the number of extrusion steps due to polymer degradation (main-chain scission). Russo et al. explain the increase from the first to the second extrusion step with cross-linking mechanisms that occur competing with main-chain scission.<sup>2</sup>

The slopes of the samples are almost 0, which is valid for unbranched linear polymers, except for the neat matrix, where the slope is reduced, indicating some kind of branching or interaction, higher network density, respectively.

#### Rheological Properties ( $G'$ , $G''$ , and $\eta^*$ vs. $\omega$ ) of PA6 as a Function of $\text{TiO}_2$ Reinforcement (7 vol %) as well as Extrusion Steps (0, 1, 2, 7)

Figures 3 and 4 also show the rheological behavior of nanoreinforced PA6 with 7 vol %  $\text{TiO}_2$  particle content after 1, 2, and 7 extrusion steps.

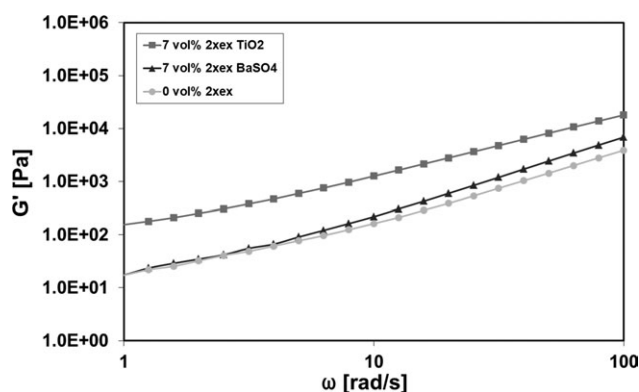


Figure 9.  $G'$  dependence on frequency for two times extruded 7 vol %  $\text{TiO}_2$  and  $\text{BaSO}_4$  masterbatches.

The addition of particles increases  $G'$  (Figure 3) of about one order of magnitude depending on the respective number of extrusion steps. Multiple extrusion leads to a decreasing  $G'$  versus  $\omega$  (Figure 3). The slope increases from extrusion step to extrusion step.

The addition of particles increases  $G''$  versus  $\omega$  (Figure 4) only half a decade, which is less than the  $G'$ -increase. So particles do have a higher impact on elasticity compared with plasticity. The  $G''$  versus  $\omega$  (Figure 4) reveals a reduction of the loss modulus with increasing extrusion steps. From the first and second extrusion step, we again have the phenomenon of the same curve progression for  $G''$  versus  $\omega$ . The slopes of the different samples are slightly decreasing in contrast to a bigger decrease of the neat matrix.

In Figure 5 ( $\eta^*$  vs.  $\omega$ ), we observe that reinforcing the matrix with nanoparticles doubles the viscosity compared with neat matrix, PA6.

In Figure 5, we observe that once and twice extruded nanoparticle filled material show the same viscosity range going down by 50% after seven extrusion steps. The slopes of the samples are almost 0, which is valid for unbranched linear polymers, lower density networks, respectively.

The reinforcement of PA6 with nanocomposites increases the moduli and viscosity due to the dominance of intrinsic friction over the not relevant molecular reorganization.<sup>28</sup>

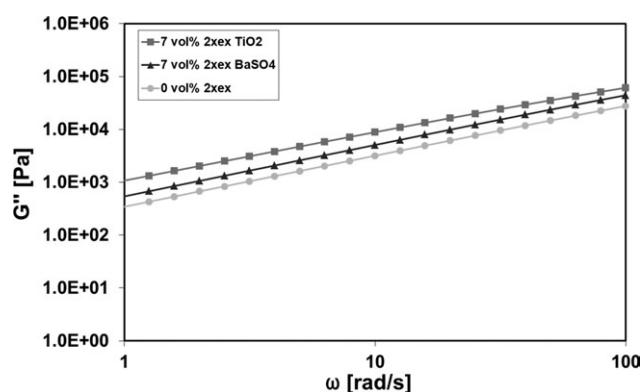
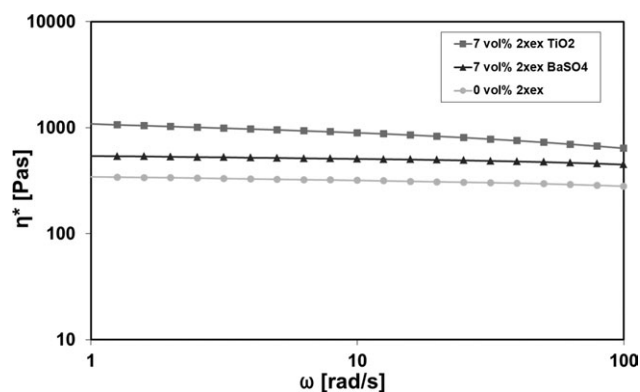


Figure 10.  $G''$  dependence on frequency for two times extruded 7 vol %  $\text{TiO}_2$  and  $\text{BaSO}_4$  masterbatches.

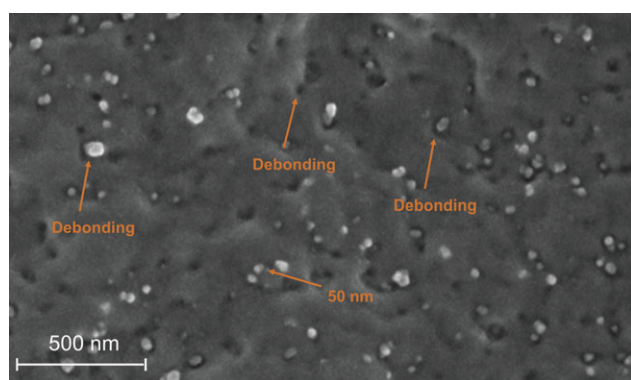


**Figure 11.** Viscosity dependence on frequency for two times extruded 7 vol % TiO<sub>2</sub> and BaSO<sub>4</sub> masterbatches.

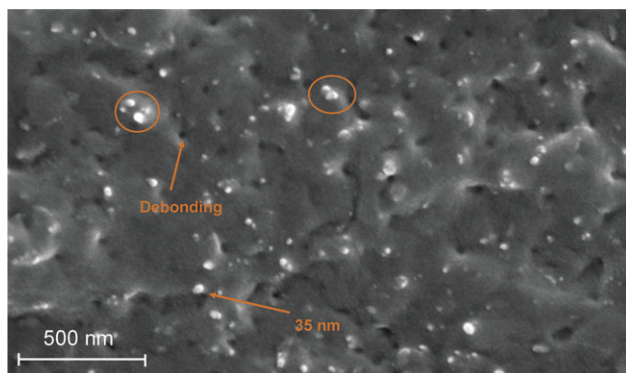
Multiple extrusion leads to a decreasing  $G'$  versus  $\omega$  (Figure 3) due to polymer degradation. Independent of the respective  $\omega$ -range the slopes run to a maximum after 7 extrusion steps, corresponding to a degradation process. Low-molecular parts are able to flow easier building up a higher degree of chemisorption and physisorption resulting in a higher intrinsic interaction. This kind of slope progression is also in accordance to dispersion index looking at Figure 2. The higher dispersion index the lower the slope ( $G'$ ).

The viscosity progression indicates that the degradation of polymer matrix overweighs the interchanges between particles and matrix. Russo et al. have reported an increase in shear thinning behavior for multiple extruded clay nanocomposites with respect to once extruded material,<sup>2</sup> explaining this with an improved silicate dispersion.

The thermal stability of the materials can be improved by nanoparticles, too.<sup>29,30</sup> The thermal stability is in comparison with neat matrix reduced due to polymer degradation as a function of extrusion steps. Nanoparticle deagglomeration from the first to the second extrusion step does not lead to an improved particle-matrix interaction, due to a missing reduction in slope (Figure 5;  $\eta^*$  vs.  $\omega$ ). According to literature, the effect of poly-



**Figure 12.** High magnification SEM images of BaSO<sub>4</sub> nanoparticles embedded in a PA6 matrix. Arrows highlight debonding. [Color figure can be viewed in the online issue, which is available at wileyonlinelibrary.com.]



**Figure 13.** High magnification SEM images of TiO<sub>2</sub> nanoparticles well embedded in a PA6 matrix (highlighted via circles). Arrows highlight debonding. [Color figure can be viewed in the online issue, which is available at wileyonlinelibrary.com.]

mer-particle interaction is more evident in the low frequency range.<sup>21,22</sup> An improved degree of deagglomeration and stronger matrix-filler interactions will have a strong impact on rheology. The viscosity increases due to the set-up of a three-dimensional network of dispersed particles but slope decreases due to remaining agglomerates in the masterbatch.

#### Rheological Properties ( $G'$ , $G''$ , $\eta^*$ , vs. $\omega$ ) of Reinforced PA6: 7 vol % TiO<sub>2</sub> and BaSO<sub>4</sub>; Twice Extruded

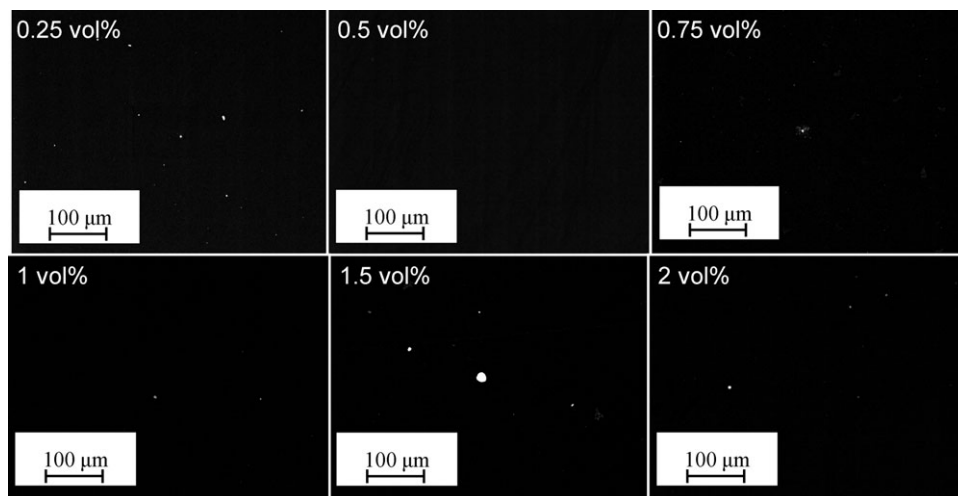
The  $G'(\omega)$  of the materials with two different kinds of nanoparticles can be seen in Figure 9. For this 7 vol % masterbatch, the nanoparticles were incorporated in a first extrusion step and dispersed in a second extrusion step. The reference without nanoparticles was extruded twice, as well. In case of BaSO<sub>4</sub>, the rheological behavior is very similar to neat matrix: Increase  $G'$  with increasing frequency. In case of TiO<sub>2</sub>,  $G'$  is by one magnitude higher especially at low frequencies. The slope for  $G'$  is higher for neat matrix and BaSO<sub>4</sub>-filled matrix than for TiO<sub>2</sub>-nanocomposites.

$G''(\omega)$  versus  $\omega$  (Figure 10) reveals that for BaSO<sub>4</sub>  $G''$  increases compared with neat, twice extruded matrix. The difference of  $G''$  between the three materials is higher at low frequencies. The slope of  $G''$  of TiO<sub>2</sub>-nanocomposites is slightly lower than neat matrix or BaSO<sub>4</sub>-filled masterbatches.

$\eta^*$  (Figure 11) of BaSO<sub>4</sub> is between TiO<sub>2</sub> filled PA 6, which is higher and neat PA 6, which is lower. The slope for BaSO<sub>4</sub> is higher (around 0) than for PA6. TiO<sub>2</sub> filled PA 6 shows the highest negative slope of these three materials.

TiO<sub>2</sub> reinforces the PA 6 matrix more than BaSO<sub>4</sub>. The slope in  $G'$  indicates a stronger interaction between TiO<sub>2</sub>-particles than for BaSO<sub>4</sub>-particles. The presence of strong interactions, for example, via hydrogen bonding, leads to an increase in  $\eta^*$ , too. Such a strong nanoparticle/polymer interaction is accompanied with a strong viscosity increase.<sup>31,32</sup> The slope for unbranched polymer without interaction is 0. The interaction in neat PA 6 due to branching is higher than in BaSO<sub>4</sub>-nanocomposites, being topped by TiO<sub>2</sub>-nanocomposites. The starting point of the viscoelastic region will take place at lower frequencies in case of TiO<sub>2</sub>-particles due to strong interactions.





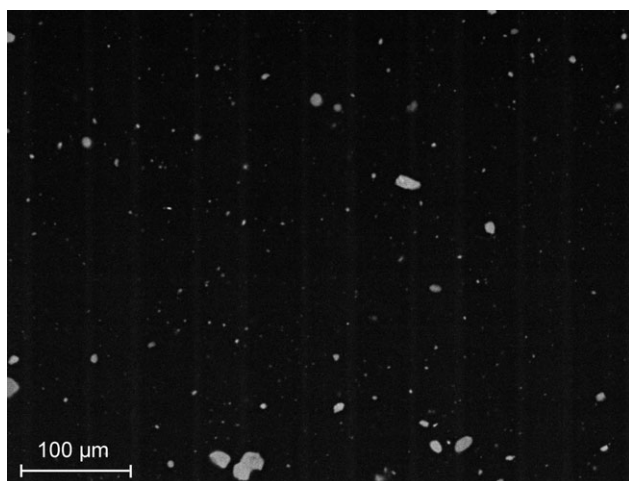
**Figure 14.** SEM images of a seven times extruded masterbatch diluted in an eighth extrusion steps down to 0.25, 0.5, 0.75, 1, 1.5, 2 vol %.

Looking at SEM images (Figures 12 and 13), it is very impressive in case of  $\text{TiO}_2$  to see a good particle-matrix interaction (well embedded particles!) versus a bad (“debonding”) particle-matrix interaction in case of  $\text{BaSO}_4$ . This kind of behavior can be well detected via online viscosity check ( $G'$ ,  $G''$ ,  $\eta^*$ , slope deviation), for example, in a bypass or a die configuration, device, respectively, with pressure detection.

#### Rheological Properties ( $G'$ , $G''$ , $\eta^*$ , vs. $\omega$ ) of $\text{TiO}_2$ Reinforced PA6 (0, 1, 2, 7 vol %); Twice Extruded

Two masterbatches of with 7 vol % particle content were taken to perform further extrusion steps. In this extrusion step, neat PA 6 was added (“dilution step”) to realize lower particle loading. This procedure was performed with:

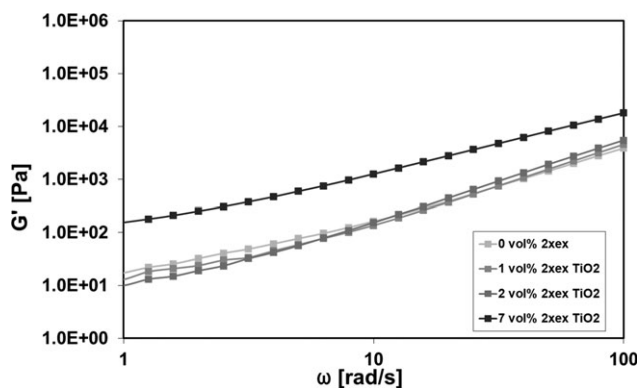
1. Original masterbatch after compounding particles and matrix, thus once extruded.
2. Masterbatch, compounded and six times dispersed, thus seven times extruded.



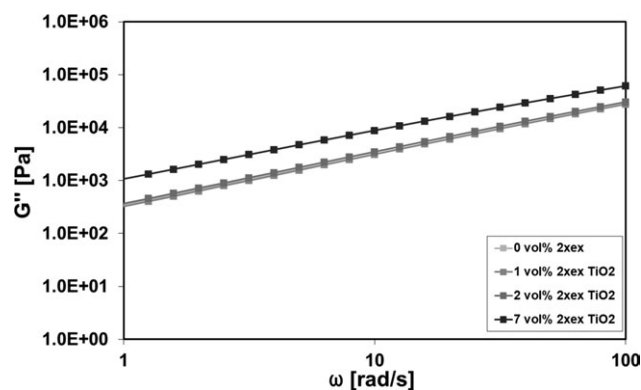
**Figure 15.** SEM image of 7 vol %  $\text{TiO}_2$  PA6 masterbatch after two extrusion steps.

These materials were taken for one further dilution step. The labeling is as follows: the masterbatch diluted in a second step after the first compounding is referred as two times extruded, even though only the masterbatch fraction is extruded twice. The fraction of the added neat PA 6 is only extruded once. The masterbatch, which is dispersed six times after compounding and is then diluted, is referred to as eight times extruded. Here again, the needed neat PA6 for the dilution is only extruded once, the masterbatch part is extruded eight times.

From the SEM and  $\mu$ -CT-analysis, a deagglomeration of the respective agglomerates is evident but we will never be able to destroy all the agglomerates independent of the number of extrusion steps we apply. Figure 14 shows the state of the art of agglomerates after 8 times of extrusion, the so called dilution steps, to realize the final particle content. Even here we see remaining agglomerates which might be the reason for a lower impact strength in case of reinforced PA 6.<sup>25</sup> For the 7 vol % masterbatch after two extrusion steps, analyzed rheologically, a dispersion index of  $D = 0.88$  according to eq. (1) is reached (Figure 15). The dispersion index of lower particle contents is smaller.



**Figure 16.** Curve progression of  $G'$  as function of frequency for different  $\text{TiO}_2$  filler contents in a PA6 matrix incorporated in a first extrusion steps and diluted in a second extrusion step.



**Figure 17.**  $G'$  as function of frequency for different  $\text{TiO}_2$  filler contents in a PA6 matrix incorporated in a first extrusion steps and diluted in a second extrusion step down to 1, 2, and 7 vol %.

The rheological properties are measured for the once extruded and for the diluted materials (2xex: 2nd extrusion step). The order of  $G'(\omega)$  (Figure 16) for different particle loadings is a function of applied frequency. From 1 to 10 Hz the storage modulus decreases slightly with increasing particle content (0–2 vol %) but increases about one decade for 7 vol %. Starting from 10 Hz,  $G'$  increases with increasing particle content.

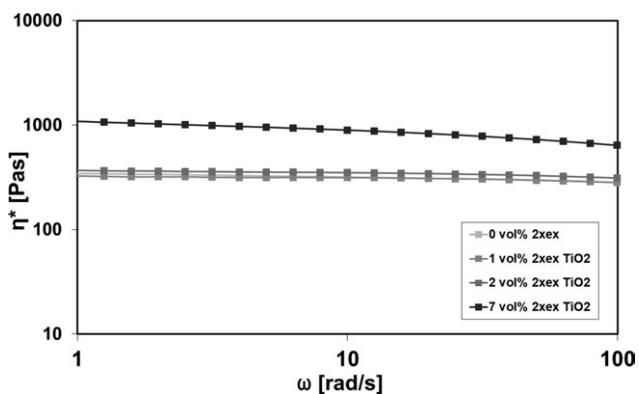
$G''(\omega)$  (Figure 17) is almost the same over the whole frequency range for low filler contents (0–2 vol %). For 7 vol % nanoparticle filled PA 6,  $G''$  increases half a decade at low frequencies and as the slope of  $G''$  for the 7 vol % masterbatch is smaller, the distance between the graphs decreases.

$\eta^*(\omega)$  (Figure 18) is slightly increased with small nanoparticle loading. With higher loading, the viscosity is increased half a decade decreasing with higher frequency.

The higher the particle content, the steeper is the  $G'$ -curve except at high volume fractions. At low frequencies, the effect of interaction and filler content is more evident due to the potential of polymer flowing and therefore increasing of particle–matrix interaction.<sup>21</sup> This reveals a particle–particle network occurring at higher frequencies which will be reduced by the polymer flowing at low frequencies. The particle–particle network is more important at higher loadings but only up to a certain amount due to the potential increase of agglomerates. The increase in  $\eta^*$  is also found in Ref. 2. Thus, the slope of  $\eta^*$  of highly filled nanocomposites is smaller than of lowly filled compounds having almost a slope of 0. The increase of viscosity with particle loading reveals that the nanocomposites do not attain a pseudo solid-like behavior through a three-dimensional superstructure. In Refs. 4–6 and 33, it is shown that the slope in the low frequency viscoelastic range decreases with organoclay loading, which indicates that the nanocomposites attained a pseudo solid-like behavior due to the nano-reinforcing effect of the clay. The higher the  $G'$  and the smaller the slope (at low frequency (In Ref. 6, it is  $\omega < 0.1$ )), the more pronounced the interaction between the silicate platelets and their tendency to form a three-dimensional superstructure/solid like behavior.<sup>4–6</sup>

## CONCLUSIONS

In this article, PA 6-nanocomposites reinforced with  $\text{TiO}_2$  and  $\text{BaSO}_4$  nanoparticles were analyzed rheologically as well as opti-



**Figure 18.** Viscosity as function of frequency for different  $\text{TiO}_2$  filler contents in a PA6 matrix incorporated in a first extrusion steps and diluted in a second extrusion step.

cally. So far, it is evident that the respective interchanges polymer-particle as a function of molecular weights as well as degree of deagglomeration can be characterized via the measurement of rheological properties ( $G'$ ,  $G''$ ,  $\eta^*$  vs.  $\omega$ ) especially in the low frequency range. The results can be summarized as follows:

1. Deagglomeration due to multiple extrusion does not lead to a change of the rheological properties ( $G'$ ,  $G''$ ).
2. Extrusion steps lead to a decrease in rheological properties and viscosity ( $G'$ ,  $G''$ ,  $\eta$ ).
3. At lower frequencies, the differences in rheological properties ( $G'$ ,  $G''$ ) are of higher magnitude than at higher frequencies.
4.  $\text{TiO}_2$  is a better reinforcing filler than  $\text{BaSO}_4$ .  $G'$  is one magnitude increased for  $\text{TiO}_2$ .  $G''$  is increased, but less than  $G'$  for  $\text{TiO}_2$  compared with  $\text{BaSO}_4$ . The viscosity is more increased by  $\text{TiO}_2$  than for  $\text{BaSO}_4$ .
5. The interaction of  $\text{TiO}_2$  with matrix is bigger than in case of  $\text{BaSO}_4$ . This can be seen in a smaller slope for  $\text{TiO}_2$  especially for  $G'$  in the lower frequency region.
6. The remaining agglomerates seem to act as defects decreasing the energy absorption of the compound.<sup>25</sup>
7. A particle–particle network depended on particle loading and agglomeration can be found. The slope in the small frequency region for  $G'$  and  $G''$  is decreased for higher particle loadings and increased after two and three extrusion steps. In case of multiple extruding, a network will be build up, as the slope is reduced again.

## ACKNOWLEDGMENTS

The authors gratefully acknowledge the support of the German Federal Ministry of Education and Research (BMBF) (Contract no. 03X0058C) and the Center for Project Management (PTJ) for funding this research project.

## REFERENCES

1. Karger-Kocsis, J.; Zhang, Z. In *Mechanical Properties of Polymers Based on Nanostructure and Morphology*; Baltà-Calleja, J. F.; Michler, G., Eds.; Taylor and Francis Group:

- Boca Raton, London, New York, Singapore, **2005**; pp 565–641.
2. Russo, G. M.; Nicolais, V.; Di Maio, L.; Montensano, S.; Incarnato, L. *Polym. Degrad. Stab.* **2007**, *92*, 1925.
  3. Michler, G. H. In *Mechanical Properties of Polymers Based on Nanostructure and Morphology*; Baltà-Calleja, J. F.; Michler, G., Eds; Taylor and Francis Group: Boca Raton, London, New York, Singapore, **2005**; pp 393–446.
  4. Chow, W. S.; Ishak, Z. A. M.; Karger-Kocsis, J. *Macromol. Mater. Eng.* **2005**, *290*, 122.
  5. Krishnamoorti, R.; Giannelis, E. P. *Macromolecules* **1997**, *30*, 4097.
  6. Lee, K. M.; Han, C. D. *Macromolecules* **2003**, *36*, 7165.
  7. Hui, S.; Chaki, T. K.; Chattopadhyay, S. *Polym. Compos.* **2010**, *31*, 377.
  8. Giannelis, E. P.; Krishnamoorti, R.; Manias E. In *Advances in Polymer Science: Polymer-Silicate Nanocomposites*; Abe, A.; Albertsson, A.-C.; Dusek, K.; de Jeu, W. H.; Kobayashi, S.; Lee, K.-S.; Leibler, L.; Long, T. E.; Manners, I.; Möller, M.; Terentjev, E. M.; Voit, B.; Wegner, G.; Wiesner, U.; Vicent, M. J.; Genzer, J., Eds.; Springer: Berlin, **1999**; Vol. 138, pp 107–147.
  9. Kharchenko, S. B.; Douglas, J. F.; Obrzut, J.; Grulka, E. A.; Migler, K. B. *Nat. Mater.* **2004**, *3*, 564.
  10. Ren, J.; Krishnamoorti, R. *Macromolecules* **2003**, *36*, 4443.
  11. Hoffmann, B. Ph.D. Thesis, University of Freiburg, Freiburg, Germany, **2000**.
  12. Privalko, V. P.; Shumsky, V. F.; Privalko, E. G.; Karaman, V. M.; Walter, R.; Friedrich, K.; Zhang, M. Q.; Rong, M. Z. *Sci. Technol. Adv. Mater.* **2002**, *3*, 111.
  13. Bretas, R. E. S.; Powell, R. L. *Rheol. Acta* **1985**, *24*, 69.
  14. Minagawa, N.; White, J. L. *Polym. Eng. Sci.* **1975**, *15*, 825.
  15. Minagawa, N.; White, J. L. *J. Appl. Polym.* **1976**, *20*, 501.
  16. Friedrich, C. J. *J. Appl. Polym. Sci.* **1995**, *57*, 499.
  17. Jain, S.; Goossens, J. G. P.; Peters, G. W. M.; van Duin, M.; Lamstra, P. J. *Soft Matter* **2008**, *4*, 1848.
  18. Hoffmann, B.; Kressler, J.; Stöppelmann, G.; Friedrich, C.; Kim, G.-M. *Colloid Polym. Sci.* **2000**, *278*, 629.
  19. Han, C. D.; John, M. S. *J. Appl. Polym. Sci.* **1986**, *32*, 3809.
  20. Han, C. D.; Kim, J. K. *Macromolecules* **1989**, *2*, 4292.
  21. Lee, K. M.; Han, C. D. *Macromolecules* **2003**, *36*, 7165.
  22. Jian, L.; Zhou, C.; Gang, W.; Wei, Y.; Ying, T.; Qing, L. *Polym. Compos.* **2003**, *24*, 323.
  23. Knör, N. F. Ph. D. Thesis, Institut für Verbundwerkstoffe GmbH, Kaiserslautern, Germany, **2010**.
  24. Villmow, T.; Pötschke, P.; Pegel, S.; Häusler, L.; Kretzschmar, B. *Polymer* **2008**, *49*, 3500.
  25. Hassinger, I.; Burkhart, T. J. *Thermoplast. Compos. Mater.*, **2012**, *25*, 573.
  26. Knör, N.; Schröck, W.; Hauptert, F.; Schlarb, A. K. In *2nd Vienna International Conference, Vienna, Austria, March 14–16, 2007*; Vol. 2, pp 283–288.
  27. Bartczak, Z.; Argon, A. S.; Cohen, R. E.; Weinberg, M. *Polymer* **1999**, *40*, 2347.
  28. Markov, A. V. *Materialwiss. Werkst.* **2008**, *39*, 227.
  29. Kusmono, Ishak, Z. A.; Chow, M. W. S.; Takeichi, T.; Rochmadi. *eXPRESS Polym. Lett.* **2008**, *2*, 655.
  30. Khumalo, V. M.; Karger-Kocsis, J.; Thomann, R. *eXPRESS Polym. Lett.* **2010**, *4*, 264.
  31. Gahleitner, M.; Kretzschmar, B.; Van Vliet, G.; Devaux, J.; Pospiech, D.; Bernreitner, K.; Ingolic, E. *Rheol. Acta* **2006**, *45*, 322.
  32. Gahleitner, M.; Kretzschmar, B.; Pospiech, D.; Ingolic, E.; Reichelt, N.; Bernreitner, K. *J. Appl. Polym. Sci.* **2006**, *100*, 283.
  33. Bhatia, A.; Gupta, R. K.; Bhattacharya, S. N.; Choi, H. J. *J. Appl. Polym. Sci.* **2009**, *114*, 2837.